Int. J. Electrochem. Sci., 17 **(2022)** Article Number: 220853, doi: 10.20964/2022.08.56

International Journal of
ELECTROCHEMICAL
SCIENCE
www.electrochemsci.org

Influence of Internal Chloride and Cracking on the Corrosion Behavior of Steel in Mortar

Tian Yupeng, Jiuwen Bao, Peng Zhang[*], *Tiejun Zhao*

Center for Durability & Sustainability Studies of Shandong Province, Qingdao University of Technology, Qingdao 266033, PR China
[*]E-mail: peng.zhang@qut.edu.cn

Received: 1 April 2022 / *Accepted:* 13 June 2022 / *Published:* 4 July 2022

Chloride-induced steel corrosion has been identified as the major reason for the durability deterioration of reinforced concrete structures in the marine environment. In this paper, the influence of internal chloride content and the cracking on corrosion behavior of carbon steel in mortar was experimentally investigated. First, the corrosion behavior of carbon steel embedded in an ordinary mortar containing different chloride content (ranging from 0 to 0.6% vs. binder mass) below the chloride threshold level was characterized by electrochemical impedance spectroscopy (EIS) and corrosion potential measurement. In terms of the cracking, corrosion behavior of carbon steel embedded in cracked mortar subjected to different exposure environments of air, water dry-wet cycles, and NaCl solution dry-wet cycles were reflected by corrosion potential measurement. The obtained results indicate that low chloride content does not influence the final passivation degree and polarization resistance of steel in mortar. However, when mortar is exposed to a humid environment, the activity of rebar is noticeably improved. Under the coupled action of cracking and dry-wet cycles, the corrosion rate of carbon steel in mortar sample increase with the increase of crack width. Once the cracked mortar is exposed to NaCl solution, even a tiny crack width increases the corrosion risk of Carbon steel.

Keywords: durability; Chloride attack; Steel corrosion; Crack; Dry-wet cycles

1. INTRODUCTION

Chloride-induced steel corrosion has been identified as the main reason for the durability deterioration of concrete structures in the marine environment. A characteristic feature of chloride attack, distinguished from other deterioration mechanisms, is that its primary action only acts on the steel corrosion process rather than the cement-based material matrix [1-3]. Pitting corrosion is a common result caused by chloride. The cause of pitting corrosion is that chloride ions gather locally on the surface of steel bars, which will reduce the sectional area of local reinforcing bars, resulting in a

decrease in the bearing capacity of reinforced concrete members [4, 5]. Moreover, the accumulation of corrosion products on the steel surface will exert an expansion force acting on the concrete cover, leading to cracks and spalling of the concrete cover [6-10].

When steel is embedded in cement-based materials, intact passivation layers are formed on the steel surface. These nano-films adhered to the steel surface are generally composed of Fe_3O_4 inner layer and γ-Fe_2O_3 outer layer. In the presence of chloride, the passive film is gradually dissolved by the concrete pore solution by forming soluble $FeCl_3$. Once the protective oxide film is disrupted, corrosion may initiate soon under the action of water and oxygen. Chloride acting as the high-performance catalyst cannot be consumed during the total corrosion process but remains available for further corrosion [3].

The main resources of chloride ions in cement-based materials are the raw materials and the service environment. Generally, the original chloride content in raw materials is low except for using chloride-contaminated aggregate, seawater, brackish water, or admixtures containing chlorides [3, 11, 12]. To limit chloride content in concrete, standards and specifications in various countries and regions generally prescribe the ultimate value, e.g., British Standard BS 8110, European Standard ENV 206, and American code ACI 318-89 [13-15]. It has been shown that steel corrosion will initiate only if the free chloride content exceeds a certain level, namely the critical chloride [16]. In terms of critical chloride, researchers have conducted much research work. The critical chloride value is influenced by different factors, such as water/binder ratio, binder type, and steel surface condition [17, 18]. According to Chen et al. [19], the critical chloride value is generally higher than 1.43% of cementitious materials. Although many research studies have been conducted to investigate the chloride-induced corrosion mechanism, very few studies concerning the influence of low chloride content below the critical chloride on steel corrosion are available. The effect of low concentration chloride ions in cement-based materials on steel corrosion is still unclear.

In most cases, chloride-induced steel corrosion originates from the outer service environment. Prediction of chloride penetration and movement process in concrete is a research emphasis and a key element of durability design [20-22]. Numerous studies corresponding to the chloride movement mechanism have been conducted to accurately predict the chloride penetration [3, 23, 24]. To get a truer depiction of the actual situation, the coupling action of different environmental factors should be considered [25-30]. The coupling action of dry-wet cycles and chloride has been recognized as one of the most unfavorable conditions [31-33]. This is so because the dry-wet cycles can effectively promote chloride penetration. On the other hand, if concrete with an initial flaw, such as microcracks, is exposed to the marine environment or deicing salts, the coupling effect accelerates the chloride penetration by providing the available transport path [29, 34]. Accordingly, in terms of the durability design and service life prediction, the actual service life of the concrete structure may be overestimated without considering the influence of cracks, resulting in premature deterioration of concrete structure [35, 36].

This paper aims to investigate the effect of internal chloride attack and cracking on the corrosion behavior of carbon steel in ordinary mortar specimens. First, for the internal chloride attack, the corrosion behavior of carbon steel was studied after directly adding NaCl into the fresh mortar. The maximum chloride ion content is 0.6% below the critical chloride content. The corrosion potential and

polarization resistance of the carbon steel were regularly measured to reflect the state of the carbon corrosion. The effect of crack width under different exposure conditions on the steel corrosion was obtained by corrosion potential measurement.

2. MATERIALS AND METHODS

2.1. Mixture and materials

Binder used in this study is Type I Portland cement manufactured by Shanshui Company in Qingdao, China. The chemical composition of cement is listed in Table 1. Both sand and water used in the study were locally available in Qingdao. For each mortar sample, two steel bars were embedded – one is class Q235 plain round carbon steel with 8 mm diameter and 170 mm length, while the other one was class 305L stainless steel conforming to the GB/13013-1991 standard in China with a 4 mm diameter and 170 mm length. Carbon steel and stainless steel were used as the working electrode and the reference electrode for the corrosion potential measurement and EIS testing, respectively. A polycarboxylic admixture was used as a water reducer in the mix. In this study, two types of mortars with the water-binder ratios of 0.4 and 0.55 were prepared. Some samples were incorporated with NaCl during casting to prepare mortar samples containing different chloride content. The chloride content is 0%, 0.1%, 0.2%, 0.4%, and 0.6% by weight of cement. The mixture proportion of mortar samples in detail is listed in Table 2.

Table 1. Chemical composition of cement and fly ash(%)

Chemical composition	CaO	SiO_2	Fe_2O_3	C_3A	SO_3	K_2O	TiO_2	Na_2O
Cement	1.83	58.10	3.76	-	0.51	1.51	1.57	0.36

Table 2. Mixture proportion of mortar samples

W/b	Cl^- vs. binder (%)	Cement (kg/m^3)	Sand (kg/m^3)	Water (kg/m^3)	Superplasticizer vs. binder (%)
0.4	0%/ 0.1%, 0.2%, 0.4%, 0.6%	562	1350	300	0.2%
0.55		515	1350	283	-

Samples mixed with NaCl were used to study the influence of internal chloride attack on the corrosion potential of steel, and some unreinforced samples were used to prepare samples with different crack widths. The pretreatment, exposure condition, and experiment are shown in Figure 1.

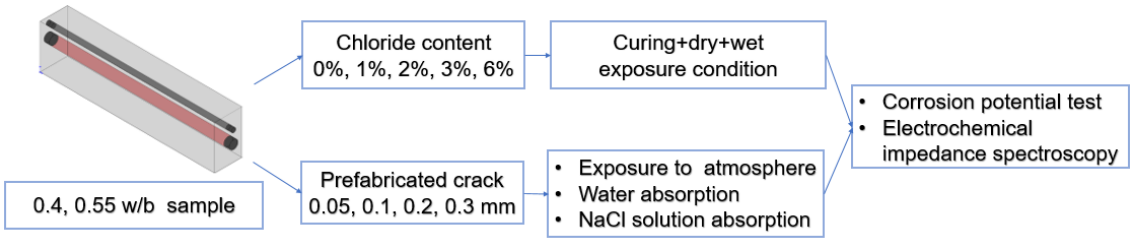

Figure 1. The pretreatment, exposure condition, and testing of the mortar samples with different internal chloride content and crack width.

2.2. Pretreatment of steels and preparation of samples

The commonly used steels are always covered by a layer of visible rust or a protective oil coating, which may interfere with the test results. In order to remove this thin rust or preservative oil layer, carbon steel and stainless steel were washed with low-concentration sulfuric acid solution and then polished with emery paper. Then, both the carbon steel and the stainless steel surfaces were cleaned with ethanol. Following the above steps, wires were separately welded at the end of the carbon steel and the stainless steel for connecting the corrosion potential measurement device. In order to avoid the occurrence of corrosion in the welding area, epoxy resin and insulating tape were applied to seal the welding area. Before the pouring process, carbon steel and stainless steel were symmetrically placed as longitudinal bars in a steel mold. In terms of fixing position in the sample, the carbon steel was embedded in a close position 1 cm away from the stainless steel to eliminate the influence of diffusion current [37, 38].

In this study, all samples with an identical dimension of 160 mm × 40 mm × 25 mm were prepared. The schematic of the specimen and steel fixing position in detail is shown in Figure 2. After one day of molding, all samples were placed in the standard curing chamber with a constant curing temperature of 20 ± 3 °C and relative humidity above 95% for 14 days.

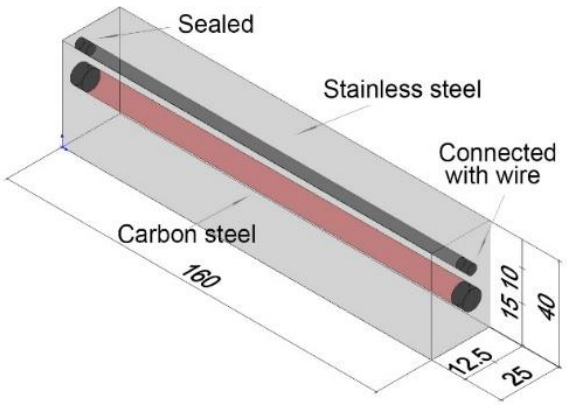

Figure 2. Schematic of specimen and installation location of carbon steel and stainless steel (mm)

2.3. Prefabricated crack

Samples with 0.55 w/b also were used to prefabricate the cracked samples. The cracks were generated on the back surface of samples (160 mm×25 mm) by three-point bending tests, as shown in Figure 3. Nominal 'target' width of crack was divided into four classes: 0.05 mm, 0.1 mm, 0.2 mm and 0.3 mm. Using a digital microscope, one transverse fissure close to the design width for each sample was screened out.

(a) Three-point bending test

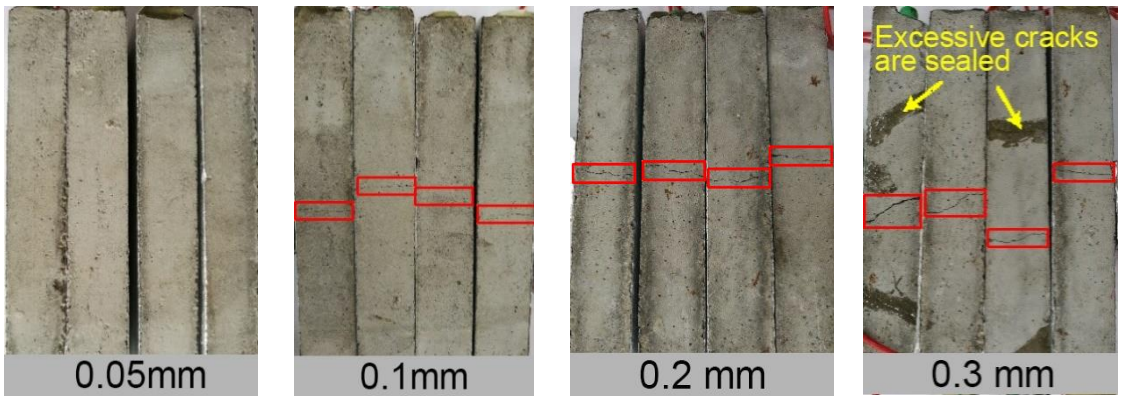

(b) The crack widths of a mortar samples

Figure 3. Prefabricated cracks by three-point bending test and crack width of the mortar samples

Later, the other remaining cracks were sealed by epoxy resin. The obtained crack widths in different exposure environments are listed in Table 3. After the cracks were generated, except for the surface with cracks and its opposite side, the other four sides of the sample were sealed using aluminum foil tape. Herein, the group without cracks was designated as the control group.

Table 3. The nominal width and actual crack width of samples in three exposure conditions of NaCl solution, water, and air. (mm)

Design widths	NaCl	Water	Air
0.05	0.049	0.047	0.071
	0.046	0.069	0.060
	0.054	0.050	0.072
0.1	0.102	0.085	0.087
	0.108	0.121	0.097
	0.109	0.127	0.115
0.2	0.247	0.235	0.172
	0.228	0.207	0.234

	0.182	0.185	0.169
	0.287	0.25	0.289
0.3	0.252	0.294	0.269
	0.265	0.421	0.310

2.4. Corrosion potential measurement

The corrosion potential between carbon steel as the working electrode and stainless steel as the reference electrode was obtained through a voltmeter. During the initial 14 days, the specimens were cured at 20 ± 3 °C and above 95% relative humidity. Then, until 80 days, the specimens were exposed to a dry condition at a temperature of 20 ± 3 °C and relative humidity around 60 ± 3%. The samples were placed in the curing condition again for the remaining test time. The initial potential was detected after removing the mold and before putting it into a standard curing chamber. Subsequently, the potential value was continually tested every day during the initial week. Later, the tested frequency intervals were 3, 5, and 10 days. For the corrosion potential of steel embedded in cracked specimens, the test interval was 7 days.

2.5. Polarization resistance by EIS

Electrochemical impedance spectroscopy (EIS) is a reliable method for determining the steel corrosion rate [39, 40]. According to the simulation results concerning the Nyquist plot date of EIS, the polarization resistance of carbon steel was obtained [5, 37]. In this investigation, the embedded stainless steel was used as the counter electrode, and a saturated calomel electrode (SCE) was employed as the reference electrode. EIS measurement was performed periodically using a sinusoidal voltage interference signal with an amplitude of 10 mV and a frequency range of 10^5Hz ~ 10^{-2}Hz. The specimens were tested at 14 days, 40 days, and 90 days after molding under a constant room temperature of 20 ± 3 °C.

2.6. Steel corrosion potential in cracked mortar exposed to NaCl solution, water, and air.

Samples with similar nominal crack widths ranging from 0 to 0.3 mm were divided into three groups. The first group was used for NaCl solution capillary absorption. Before the capillary absorption test, all other surfaces except for the exposed surface, which was the side face of the sample, were sealed with epoxy resin to ensure uni-dimensional diffusion. The cracked surface of the samples was exposed to 3% NaCl solution, and the immersion depth was within 5 ± 1 mm. The dry-wet cycles test with 6 h of absorption and 18 h of drying were carried out to accelerate the chloride migration. In this case, the Cl^-, water, and oxygen were sufficient for corrosion of carbon steel.

The second group of samples was also used for water capillary absorption, for which the procedure and device were the same as the NaCl solution capillary absorption. Here, water and oxygen were sufficient for steel corrosion. The NaCl solution or water capillary absorption process is shown in Figure 4.

Lastly, the third group of the samples was exposed to a dry environment at 20 ℃ and 50% RH. After the initiation of the experiment, corrosion potential of all three groups between the carbon steel and stainless steel was measured every 7 cycles.

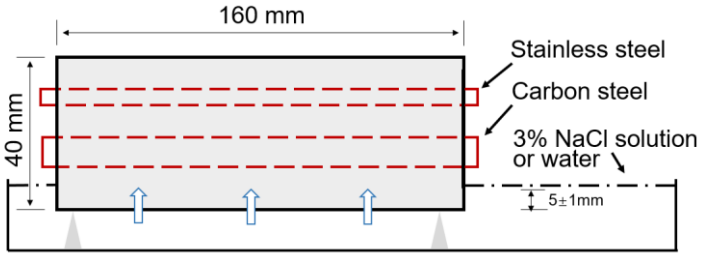

Figure 4. Schematic diagram of capillary salt or water absorption

3. RESULTS AND DISCUSSION

3.1. The steel corrosion potential in mortar with different chloride content

Corrosion potential is used as the damage index to analyze the steel corrosion degree and rate of concrete [41]. If the carbon steel is used as corrosion anode and the stainless steel as corrosion cathode, a more negative potential indicates a higher corrosion risk of the tested carbon steel. In this study, the corrosion behavior of carbon steel in mortar is evaluated by corrosion potential testing. The mechanism of chloride altering the steel corrosion potential is shown in Figure 5. With the increase in chloride concentration on the steel surface, the passive film of steel is continually dissolved into the pore solution by forming soluble salts.

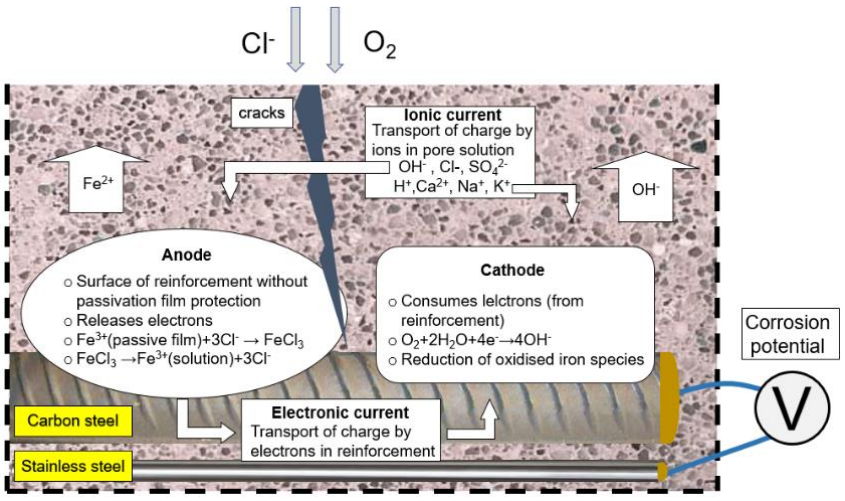

Figure 5. Schematic diagram of the steel corrosion process and half-potential test.

At the corrosion initiation, local steel without passive film is relatively active compared to other passivation areas. This activity difference leads to a potential difference between the local steel

without passive film and the passive steel in other positions, forming a micro-battery corrosion system. With the development of the chloride-induced corrosion process, the passive film gradually dissolves, and the overall steel activity increases progressively. Since stainless steel activity hardly changes, the activity difference between carbon steel and stainless steel is gradually apparent. The potential difference between the carbon steel and the stainless steel can be measured by the half-potential method, namely the corrosion potential, to characterize the gradual corrosion process of steel.

The evolution of the corrosion potential of carbon steel in mortar containing different chloride contents as a function of time is shown in Figure 6. It shows that at the beginning of the test, the initial corrosion potential is decreased with the increase of chloride concentration. In addition, less than 0.1% chloride addition exerts little influence on the initial corrosion potential. As the hydration progresses, the corrosion potential of all samples increases, which is primarily due to the gradual formation of the passive film. When the hydration is completed at around 30d, the corrosion potential values are similar for all samples, indicating that low content chloride in mortars does not affect the passive film. However, when the samples are placed in a moist environment, the curves of corrosion potential exhibit a downward trend and, at last, reach a relatively stable level. The higher the chloride content, the lower the final stable potential. For 0.4 w/b samples, the potential of steel in 0.6% mortar is finally stabilized at around – 150 mV. When the chloride content is 0.2%, the potential is over -100 mV. In addition, when the chloride content is lower than 0.1%, the potential is higher than -50 mV. This phenomenon may be attributed to the change in chloride ion distribution caused by water ingress. Water carries the chloride ions from the mortar surface to the steel surroundings, increasing the chloride ion concentration around the reinforcement. Besides, it is observed that when the chloride content is 0.1% against the binder mass, there is a subtle changing trend in the corrosion potential for all samples during the entire testing process. A low chloride content, such as 0.1%, does not appear to induce damage to the steel passive film. This phenomenon may be associated with the chemical binding and physical absorption of chloride from the cement components and hydration products. The main chemical binding is via reaction with C_3A to form calcium chloroaluminate [3]. A similar reaction with C_4AF will produce calcium chloroferrite. Physical adsorption is highly dependent on the physical absorption action of CSH, $Ca(OH)_2$, and calcium chloroaluminate. Moreover, it has been reported that the aggregates may also reduce free chloride content in the pore solution by physical adsorption [38, 39].

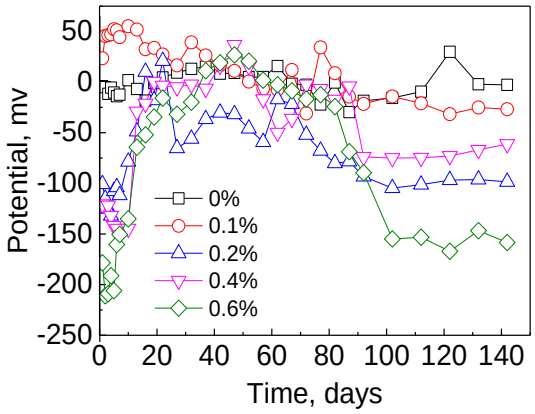

(a) 0.4 w/b mortar sample

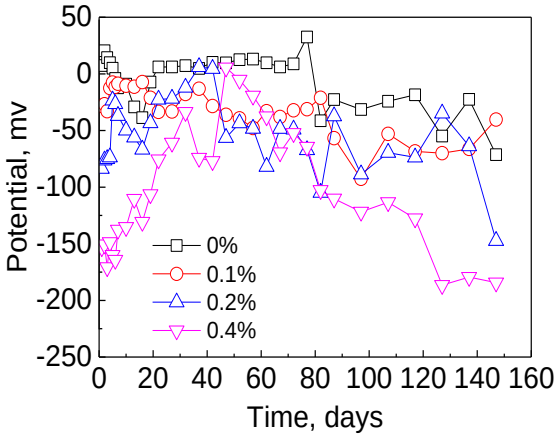

(b) 0.55 w/b mortar sample

Figure 6. The corrosion potential of steel embedded in mortar (0.4, 0.55 w/b) with chloride contents of 0%, 0.1%, 0.2%, 0.4% and 0.6%, respectively.

3.2. The steel corrosion potential in mortar under different exposure conditions

Based on the corrosion exposure environment, the corrosion potential curves in Figure 7 can be described as three stages. The first stage is till 14 days of humidity condition. The second stage is from 14 to 80 days, with specimens exposed to drying conditions. The last stage is from 80 to 140 days and is characterized by the moist condition. The first stage involves the hydration process in which the alkalinity is continually increased, leading to the gradual development of the passivation layer on the steel surface. It can be observed that the initial potential of two sets of samples at the beginning of the test is decreased with the increase of the content of chloride ions. This is most likely due to the competition between chloride and hydroxide ions [40]. Excessive chloride ions suppress the activity of the hydroxide ions; therefore, the concentration of hydroxide ions in the mortar solution is low. Thus the activity of steel is relatively high.

When the samples are placed in the drying environment, i.e., the second stage, there are two reasons for the increased tendency of corrosion potential. First, the resistance and the corrosion potential increase due to the reduced water content of mortar between the two electrodes. On the other hand, the passivation layer of steel in ordinary mortar is gradually developed. However, a slightly decreasing trend is exhibited after the potential value reaches the peak value at around 40 days. This shows that the steel has initiated to de-blunt, i.e., the protective oxide layer on the steel surface has started dissolving. Steel corrosion is an electrochemical reaction process, expressed as Equation (1).

$$Fe \rightarrow Fe^{2+} + 2e^{-} \text{ (Anode)}$$
$$O_2 + 2H_2O + 4e^{-} \rightarrow 4OH^{-} \text{ (Cathode)} \qquad (1)$$

From Equation (1), it can be seen that oxygen and water are necessary for the cathode reaction. The diffusion rate of oxygen in mortar increases with the decrease in relative humidity of mortar [41]. It is deduced that the decrease of the potential in the second stage is attributed to the replenishment of oxygen for the cathode reaction. During corrosion, oxygen is inevitably mixed into the matrix by

dissolving it in water during the mixing process. However, oxygen is gradually consumed during the corrosion process [3]. The lack of oxygen suppresses the cathode reaction of steel corrosion.

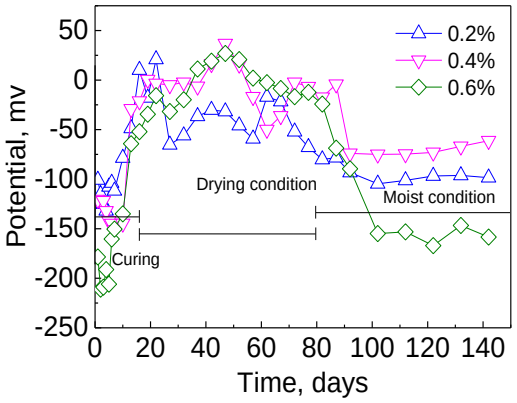

(a) 0.4 w/b mortar sample

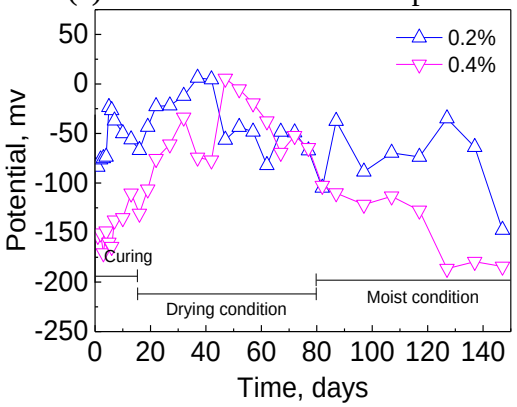

(b) 0.55 w/b mortar sample

Figure 7. The corrosion potential of steel embedded in mortar (0.4, 0.55 w/b) with chloride contents of 0.2%, 0.4% and 0.6% in different exposure environment.

Moreover, the oxygen ingress into cement-based materials is via diffusion, which is a slow process. When the samples are subjected to a moist condition in the third stage, the corrosion potential shows a rapid downward trend because the oxygen is supplemented by oxygen-contained water.

3.3. The polarization resistance of steel in the mortar containing different chloride content

EIS results of steel in 0.4 w/b mortar samples containing different chloride content are shown in Figure 8. The results of the high-frequency stage require higher water content in mortar. However, in this test, EIS is applied to the unsaturated mortar. So only the data of the impedance spectrum in the low-frequency stage, such as 1-0.01 Hz, show a good regularity, and it can be used to reflect the impedance characteristics. The low-frequency phase of the impedance spectrum is controlled by diffusion. During the polarization reaction, the oxygen around the steel is first consumed. As the reaction proceeds further, the extra oxygen will reach the steel surface from the nearby area by

diffusion driven by the electric field. The linear trend of low-frequency phase curves is observed. By comparison, it can be obtained that with the increase of chloride ion content, the slope of the frequency phase curve descends regardless of whether the mortar is incomplete-hydrated, dry, or wet. The primary reason is that extra chloride ions increase the conductivity of mortar, and the addition of chloride ions in mortar reduces the oxygen diffusion rate to a certain extent. Ideally, the high-frequency curve slope should be closed to unity. One of the possible reasons for the slope being less than unity is that the interface between mortar and electrode is rough, so the diffusion process is somewhat equivalent to a spherical diffusion [42].

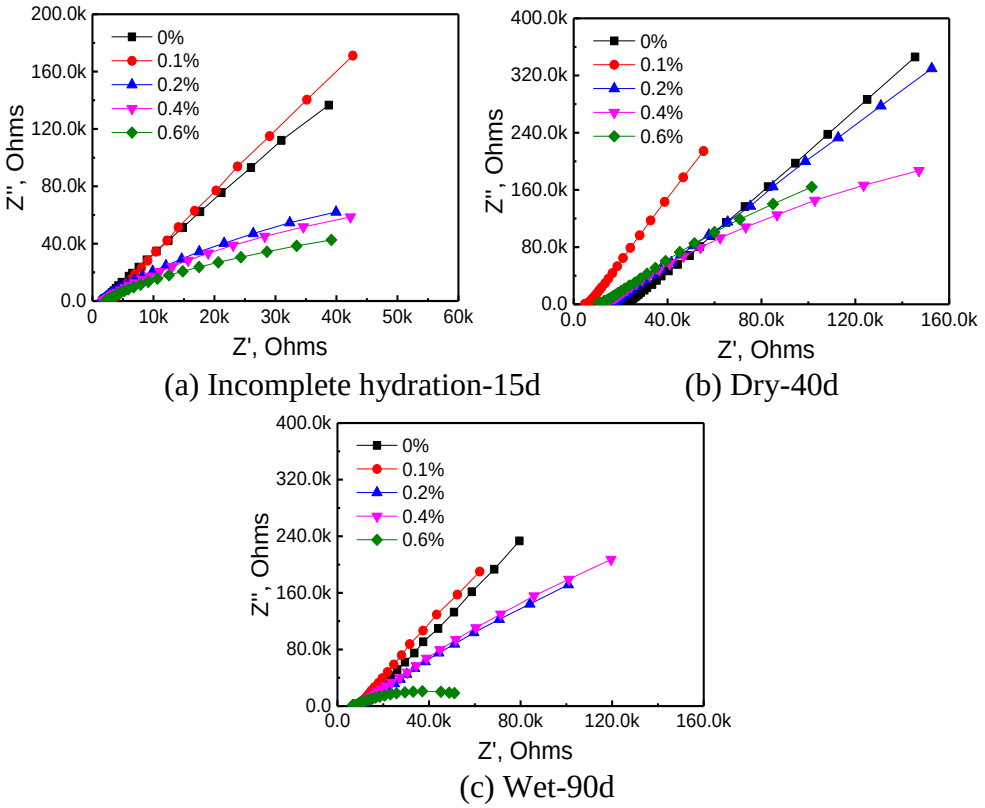

(a) Incomplete hydration-15d (b) Dry-40d

(c) Wet-90d

Figure 8. Nyquist plot diagrams of steel embedded in 0.4 w/b mortar containing chloride contents of 0%, 0.1%, 0.2%, 0.4% and 0.6% at 15d, 40d, 90d.

According to the half-potential results, the steel corrosion is not obvious no matter at 15d, 40d, or 90d. The mortar conditions appear to influence the test of the low-frequency stage of the impedance spectrum of the steel to some extent, as shown in Figure 9. Regardless of the chloride content, the dry curve is always at the left, followed by the wet curve and the incomplete hydration curve, corroborating that the mortar state affects the diffusion of oxygen in mortar.

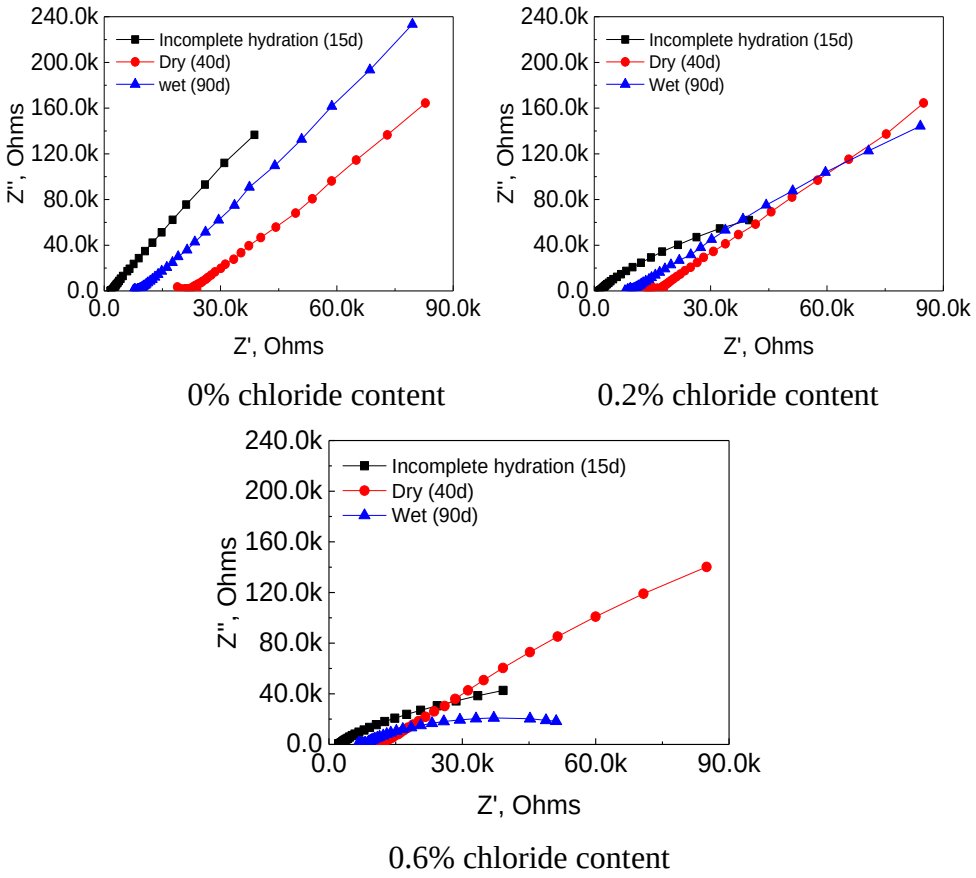

Figure 9. Nyquist plot diagrams of steel embedded in 0.4 w/b mortar containing 0%, 0.2%, 0.6% chloride content at 15d, 40d, 90d.

The accuracy of the obtained results from simulating EIS data depends on adopting a suitable equivalent electrical circuit. In this study, two hierarchical resistor-capacitance circuits, as shown in Figure 10, were selected to model the experimental impedance data. In the schematic diagram of the simple equivalent circuit, R_s denotes the solution resistance between the counter electrode and the working electrode, which makes the inevitable influence only at the highest frequencies. Q_f and R_f represent the electric behavior of the passive layer, wherein Q_f denotes the capacitance between the passive layer and pore solution, and R_f describes the polarization impedance of the passive layer. Also, Q_{dl} is used to simulate the capacitive behavior of the double layer in the pits of the steel surface. R_p is the current transfer resistance in the pits. A Warburg diffusion element Z_W is connected to reflect that the corrosion is determined by the oxygen diffusion efficiency. In the electrochemical reaction process of steel corrosion, the anode reaction occurs very quickly, while the oxygen required for the cathode reaches the steel surface through the protective layer of mortar by diffusion. Therefore, the whole corrosion process is affected by the oxygen diffusion rate. The influence of oxygen diffusion is reflected in the equivalent circuit as the Warburg impedance element. Based on the equivalent electrical circuit, the impedance of the steel-mortar system can be expressed as Equation (2).

$$Z(\omega) = R_s + \frac{R_f}{\frac{1}{1+(Z_2(\omega)/R_f)} + (j\omega R_f Q_f)^{\alpha 1}}$$

$$Z_2(\omega) = \frac{R_f}{1+(j\omega R_p Q_{dl})^{\alpha 2}} \qquad (2)$$

Where $Z(\omega)$ is the impedance of the steel-mortar system and ω is the frequency of the input electrical signal.

Equation (2) can be simplified as Equation (3)

$$Z(\omega) = Z'' - jZ' \qquad (3)$$

Where Z'' and Z' are the real and imaginary parts of the complex number, respectively.

Theoretically, when the frequency of the sinusoidal voltage signal is from zero to infinity, the relation curve forms a closed semicircle with the coordinate axis. The intersection between the curve and the axis is R_s and $2R_p + R_s$, as shown in Figure 11. More information corresponding to this equivalent circuit can be found in another study [43].

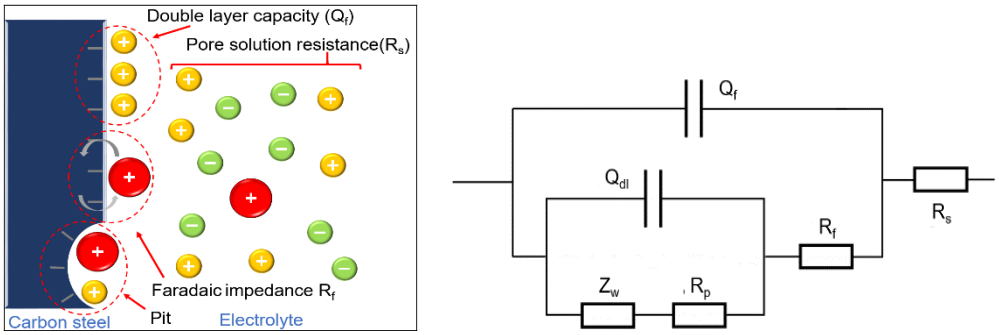

Figure 10. Equivalent electrical circuit reproducing the impedance data.

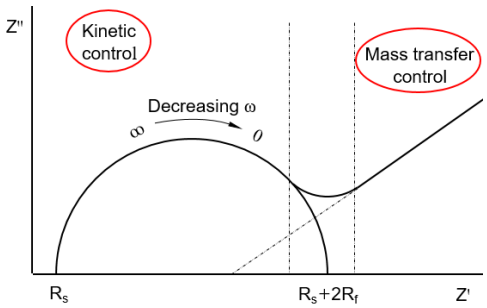

Figure 11. Theoretical Nyquist plot for the simple parallel RC circuit.

Based on Nyquist plots of EIS, the polarization resistances of carbon steel at 15, 40, and 90 days in mortar samples with different chloride content are obtained using ZSimpWin software, as shown in Figure 12. The effect of chloride decreasing the polarization resistance of steel is influenced by the mortar conditions. When the mortar is in an incomplete hydration state, chloride ion addition appears to have little effect on the polarization resistance. Figure 12 shows that when the w/b is 0.4, the effect of chloride on polarization resistance is less. Combining the result of the half-potential measurement (in Figure 6) and EIS, it is seen that the passivating film continues to be built up as hydration progresses, even in the presence of chloride ions. In the case of mortar samples exposed to

dry or wet conditions, the effects of chloride reducing the polarization resistance of the steel in the mortar are more significant. When the mortar is in a different state, the polarization resistance of the internal steel is also different. When the hydration is not completely finished, the polarization resistance of the steel is small, and the steel has been corroded. When the mortar is completely hydrated, the polarization resistance in a relatively humid environment is increased compared with that in the incomplete hydration because the passive film on the mortar surface is more complete with the increase of hydration alkalinity. When the mortar is in a dry environment, the polarization resistance further increases, and the corrosion resistance of the steel is further improved.

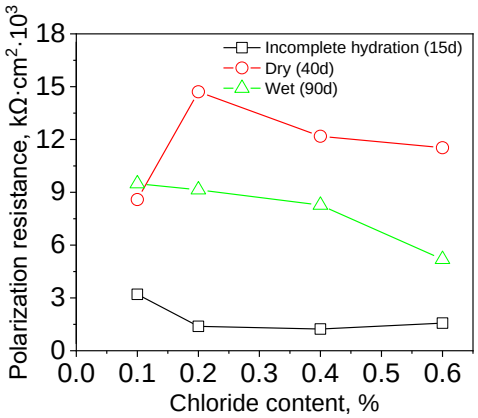

0.4 w/b mortar sample

Figure 12. The relationship between the polarization resistance and chloride content of 0.4 w/b mortar

3.4. The influence of crack width on steel corrosion potential under different exposure environments

External chloride ions originate from the outer service environment and are taken by water into the cement-based matrix. Once the chloride to hydroxide concentration ratio in the spatial domains surrounding the embedded steel is higher than the critical value, the passive film protecting the steel will be destroyed, leading to steel corrosion [44]. It has been reported earlier that the chloride diffusion rate in cracked mortar is proportional to crack width [45, 46]. In this paper, steel corrosion is highlighted by considering the crack width as the main factor influencing the corrosion process.

From Figure 13(a), it can be observed that in the atmospheric environment, even if the surface of the mortar samples is cracked, the change of potential is small. This is because the mortar around the steel is still highly alkaline, and the steel surface is still in a passive state. When the surrounding mortar is gradually carbonized to neutralize, the steel will gradually be blunted. The chloride ions ingress in the mortar is accelerated by dry-wet cycles. During the dry-wet cyclic process, chloride ions enter the mortar through the water. When the samples are dry, water migration reverses, and the water evaporates from the ends of the capillary pores open to the surrounding air. Consequently, the chloride ion concentration near the mortar surface increases. The difference in chloride ion concentration between the surface and interior will promote chloride ion diffusion.

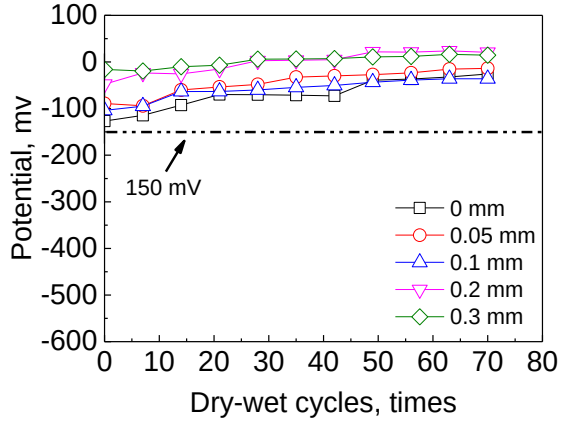

(a) Ambient air

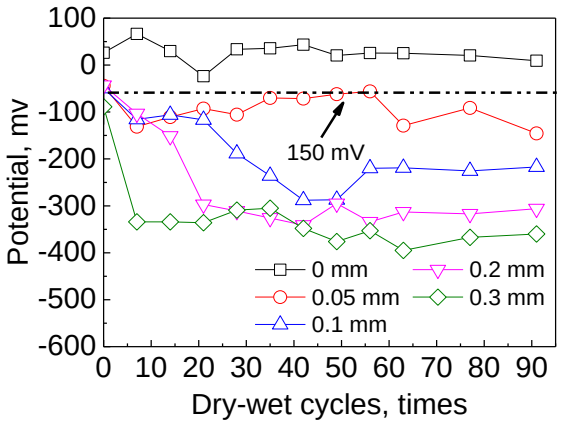

(b) Water

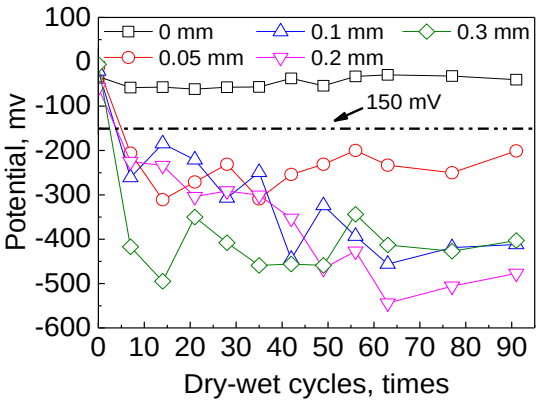

(c) NaCl solution

Figure 13. The evolution of corrosion potential of steel with different crack widths exposed to: (a) ambient air, (b) NaCl solution, and (c) water.

Figure 13 (b) and (c) indicate that with the increase in crack width, the corrosion potential is decreased under the action of dry-wet cycles. It is also observed from the dry-wet cyclic testing that the crack width of 0.05 mm has negligible effects on steel corrosion. when the carbon steel in a mortar with a 0.05 mm crack came in contact with the NaCl solution, the corrosion potential decreased significantly, as shown in Figure 13 (c). It is deduced that carbon steel in cracking mortar is vulnerable

to being attacked by chloride, even if the width of the crack is small. Additionally, the crack width affects the initiation time of corrosion. The NaCl solution reduces the corrosion initiation time more significantly compared to water. Taking samples with a uniform cracking width of 0.1 mm as an example, the corrosion potential of the samples contacted with NaCl solution reduced to -200 mV at about five dry-wet cycles, whereas the samples in contact with water took about 30 dry-wet cycles.

Figure 13 shows that although the corrosion of steel is affected by the crack width, eventually, the potential reaches equilibrium after 60 cycles. The corrosion potential indicates the corrosion degree of carbon steel. The relationship between the corrosion potential and crack width is obtained by taking the average value when the potential is stable, as shown in Figure 14. With the increase of crack width, the corrosion potential is decreased in the curve. For samples with cracks subjected to dry-wet cycles by water, the potential decreased with the increase in crack width. However, when water was replaced by a NaCl solution, the crack width above 0.1mm had a similar effect on the corrosion risk since the potential level was identical. It shows that when cracked mortar is exposed to NaCl solution, even small cracks under the action of the dry-wet cycles will expose the carbon steel to a significant risk of corrosion.

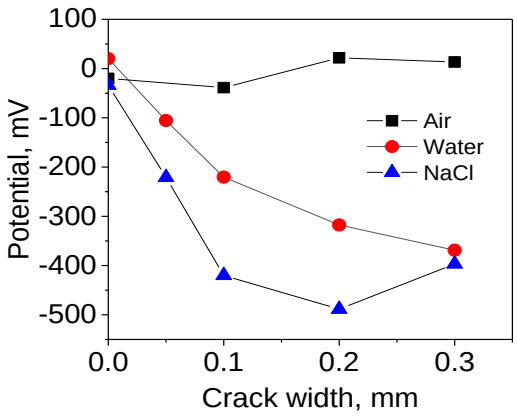

Figure 14. The relationship between the corrosion potential and crack width.

4. CONCLUSIONS

In this paper, by considering different factors, such as chloride content and crack width, the influence of chloride attack on the corrosion behavior of steel embedded in the mortar was investigated through corrosion potential and polarization resistance measurements. The following conclusions have been drawn from the experimental results and subsequent analysis.

- The chloride concentration lower than the critical chloride value does not affect the rebar activity after hydration. However, the entry of external water into the mortar promotes the influence of chloride ions on the rebar activity and polarization resistance, mainly because of the water transport the surface chloride ions to the surrounding area of the rebar. According to the half potential and impedance spectra results, the content of chloride ions lower than the critical chloride concentration

cannot cause steel bars corrosion. Nevertheless, it increases rebar activity and reduces polarization resistance.

- In terms of the external chloride attack, the coupling of cracking and dry-wet cycles can significantly promote steel corrosion. Under dry-wet cycles, the corrosion rate of carbon steel in mortar samples increases with the increase of crack width. When the cracked mortar is exposed to NaCl solution, even a small crack such as 0.05 mm will expose the carbon steel to a high corrosion risk. It seems that the NaCl solution reduces the corrosion initiation time.

References

1. Cesen, T. Kosec and A. Legat, *Corros Sci*., 75 (2013) 47.
2. P. Zhang, H. F. Wittmann, M. Vogel, S. H. Müeller and T. Zhao, *Cem. Concr. Res*., 100 (2017) 60
3. Y. Tian, P. Zhang, K. Zhao, Z. Du and T. Zhao, *Sensors,* 20 (2020) 1394.
4. W Guo, P Zhang, Y Tian, B Wang and W Ma, *Adv. Mater. Sci. Eng.,* 3 (2020) 1.
5. M. Darmawan, *Mag. Concrete. Res.*, 62 (2010) 91.
6. Y. Zhao, A. Karimi, S. Hong, B. Hu, N. Buenfeld and W. Jin, *Corros Sci*., 53 (2011) 2803.
7. Andrade, M. Keddam, R. X. Nóvoa, C. M. Pérez and H. Takenouti, *Electrochim. Acta.*, 46 (2001) 3905.
8. J Cao, Z Jin, Q Ding, C. Xiong and G. Zhang, *Constr. Build. Mater.*, 316 (2022) 125794.
9. Chen, S. Mahadevan, *Cem. Concr. Compos.*, 30 (2008) 227.
10. Z. Dong, S. Wei and P. Xing, *Corros Sci*., 53 (2011) 1322.
11. J. Xiao, C. Qiang, A. Nanni and K. Zhang, *Constr. Build. Mater.*, 155 (2017) 1101.
12. H. Yu, B. Da, H. Ma, X. Dou and Z. Wu, Constr. *Build. Mater.,* 246 (2020) 118390.
13. Structural use of concrete — patr 2 :code of practice for special circumstances. BS8100-2, 1985, British.
14. Concrete — part 1: specificatio, performance, production and conformity, Bs EN 206-1, 2000, European.
15. Building code requirements for reinforced concrete and commentary, ACI 318R-89, 1989, America.
16. U, Angst, B. Elsener, K. C. Larsen and V. Ystein, *Cem. Concr. Res.*, 39 (2019) 1122.
17. J. Bao, J. Wei, P. Zhang, Z Zhuang and T. Zhao, *Cem. Concr. Compos.*, 130 (2022) 104511.
18. S. Xue, P. Zhang, H. E. Lehmann, J. Hovind and H. F. Wittmann, *Measurement*, 183 (2021) 109882.
19. L. C. Page, *Mater. Corros.*, 60 (2015) 586.
20. P. Lambert, L. C. Page and W. R. P. Vassie, *Mater. Struct.*, 24 (1991) 351.
21. P. Zhang, D. Li, Y. Qiao, S. Zhang, C. Sun and T. Zhao, *J. Mater. Civil. Eng.*, 30 (2018) 04018265.
22. W. Wang, K. Zhao, P. Zhang, J. Bao and S. Xue, *Constr. Build. Mater.*, 267 (2021): 121008.
23. P. Zhang, D. Hou, Q. Liu, Z. Liu and J. Yu, *Cem. Concr. Res.*, (2017) S0008884617301618.
24. P. Zhang, Wang, D, Hou, Z. Liu, M. Haist and T. Zhao, *Cem. Concr. Compos.*, 78 (2017) 13.
25. J. Bao, S. Li, P. Zhang, X. Ding, S. Xue, Y. Cui and T. Zhao, *Constr. Build. Mater.*, 239 (2020) 117845.
26. Y. Wang, Y. Cao, P. Zhang, Y. Ma, T. Zhao and H. Wang, *Constr. Build. Mater.,* 209 (2019) 566.
27. J. Bao, R. Zheng, J. Wei, P. Zhang, S. Xue and Z. Liu, *J. Build. Eng.,* 51 (2022) 104273.
28. P. Lqbal, T. Ishida, Cem. Concr. Res., 39 (2009) 329.
29. Y. Li, X. Chen, L. Jin and R. Zhang, *Constr. Build. Mater.,* 127 (2016) 425.
30. J. Bao, L. Wang, *Constr. Build. Mater.,* 156 (2017) 708.
31. Z. Xu, S. Yang, W. Zhang, G. Hui and X. He, *Corros Sci*., 82 (2014) 165.
32. S. Yin, L. Jing, M. Yin and B. Wang, *Cem. Concr. Compos.*, 96 (2019) 118.

33. J. Bao, S. Xue, P. Zhang, Z Dai and Y Cui, *Struct. Concrete.*, 4 (2020) 1.
34. Q. Song, J. Bao, P. Zhang and S. Mu, *J. Mater. Sci. Technol.*, 14, (2021) 1778.
35. Poursaee, M. C. Hansson, Cem. Concr. Res., 38(2008) 1098.
36. M. Maes, D. Snoeck and N. D. Belie, *Constr. Build. Mater.,* 115 (2016) 114.
37. L. Yang, W. Sun, C. Liu, Y. Zhang and F. Liang, *J. Wuhan. Univ. Technol.*, 32 (2017) 330.
38. N. Jarrah, O. Al-Amoudi, M. Maslehuddin, A. O. Ashiru and I. A. Al-Mana, *Constr. Build. Mater.,* 9 (1995) 97.
39. Z. Chang, B. Cherry and M. Marosszeky, *Corros Sci*., 50 (2008) 3078.
40. M. Shi, Z. Chen and J. Sun, *Cem. Concr. Res.*, 29 (1999) 1689.
41. H. Ran, J. Chang and J. Wu, *Mater. Lett.*, 28(1996) 445.
42. Law, J. Cairns, *Ndt & E Int.,* 37 (2004) 381.
43. G. Vera, M. A. Climent, C. Antón, A. Hidalgo and C. Andradeera, *J. Electroanal. Chem.,* 639 (2010) 43.
44. Qiao, Harbin Institute of Technology, 2008.
45. K. Jae-Ho, R. E. Richard and N. E. Antoine, *Cem. Concr. Res.,* 29 (1999) 407.
46. C. Thong, D. Teo and C. Ng, *Constr. Build. Mater.,* 107 (2016) 172.
47. Bautista, C. J. Pomares, N. M. González and F. Velasco, *Constr. Build. Mater.,* 229 (2019) 116899.